Monte Carlo Simulations and Scattering of Electromagnetic Waves by Nanoparticles

Shashank Dattathri
#13799
UG Third Year

1 Introduction

In this project, I explore computational modeling of scattering processes in nanoscale physics. I first study Monte Carlo methods of modelling various physical systems and apply the Metropolis algorithm and variational MC to solve several problems. I then use the discrete dipole approximation code DDSCAT to solve for cross sections of scattering of electromagnetic waves by nanoparticles, and compare the results to the analytic formulae obtained by Mie theory.

2 Markov Chain Monte Carlo Methods

Analytical solutions for the Schrodinger equation are possible only for very few simple system. In most cases, one requires numerical methods in order to obtain solutions. Monte Carlo methods are used in order to obtain solutions through random sampling.
Consider a single step in a Markov chain. The current state of the system is i, and the probability of transition to the next state j is T_{ij}. For a physical system at temperature T, the transition probabilities are related by

$$\frac{T_{ij}}{T_{ji}} = \frac{P(E_j)}{P(E_i)} = \frac{e^{-\beta E_j}/Z}{e^{-\beta E_i}/Z} = e^{-\beta(E_j - E_i)} \tag{1}$$

where Z is the partition function. We note that the partition function Z is does not appear in the final expression. This is advantageous because the calculation of Z in a large system is hard.
The transition probabilities themselves are calculated using the **Metropolis algorithm**. A transition move from state i to state j is accepted with probability

$$P_a = \begin{cases} 1 & \text{if } E_j \leq E_i \\ e^{-\beta(E_j - E_i)} & \text{if } E_j > E_i \end{cases} \tag{2}$$

The system is in a random starting state, and is moved to a new random state by an allowed move at each step. Each move is accepted or rejected by the above formula.

2.1 Ising Model

The Ising model is a simple model of interacting electron spins. We consider a square N by N lattice, filled with electrons which interact only by the nearest neighbor approximation. The energy of the system is therefore given by:

$$E = \sum_{(m,n)=1} \sigma_m \sigma_n \tag{3}$$

where $(m, n) = 1$ denotes lattice points m and n which are neighbors.
This model has an exact solution. The critical temperature was given by was given by Onsager (1944):

$$T_c = \frac{2}{\ln(1+\sqrt{2})} = 2.269K \tag{4}$$

We should get a peak in the specific heat of the system at this temperature.

The Metropolis algorithm is implemented. In every step, the i^{th} electron spin is reversed, and the energy is calculated. If this reversal leads to a decrease in energy, it is accepted. Otherwise, it is accepted with probability $e^{-\Delta E/T}$. This is done for each electron in the lattice, for N sweeps. Some extra sweeps are performed to allow the system to thermalize.
After performing all the sweeps, the magnetization, energy, and specific heat were calculated according to the formulas

$$M = \left| \sum_i \sigma_i \right| \tag{5}$$

$$E = \sum_i E_i \tag{6}$$

$$c = \frac{\langle E^2 \rangle - \langle E \rangle^2}{T^2} \tag{7}$$

We see that

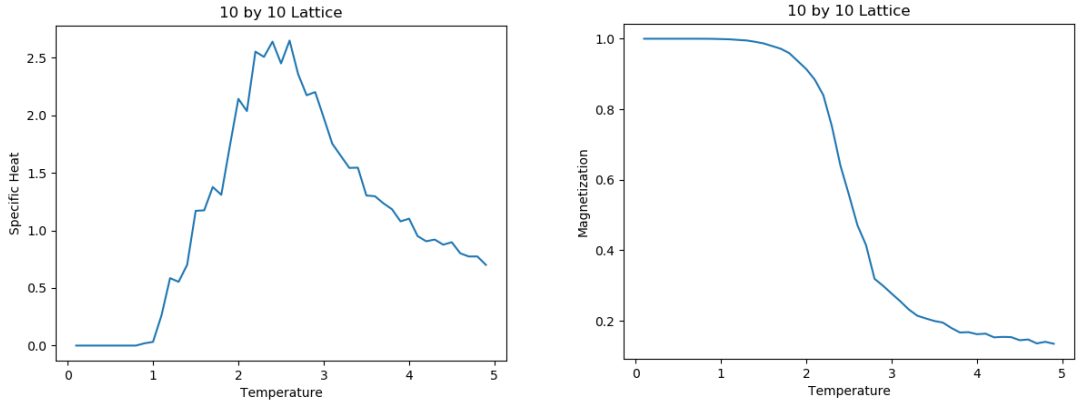

Figure 1: Specific heat and magnetization in a 10 by 10 lattice.

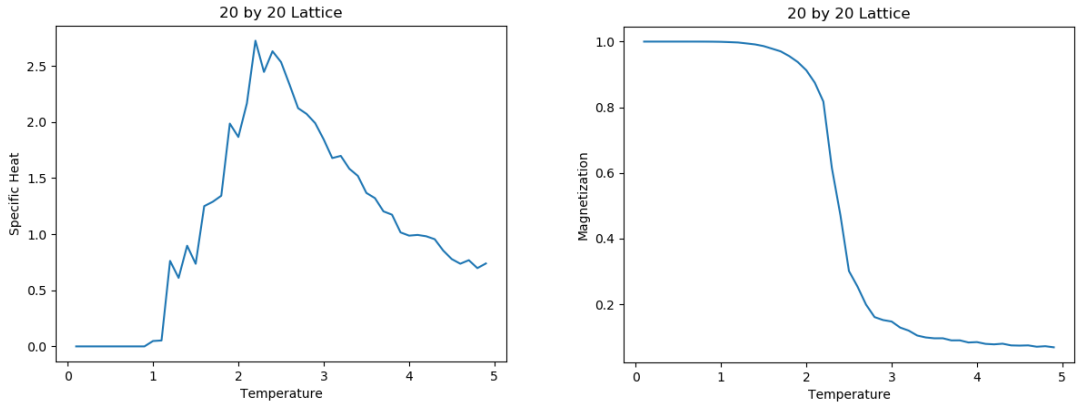

Figure 2: Specific heat and magnetization in a 20 by 20 lattice.

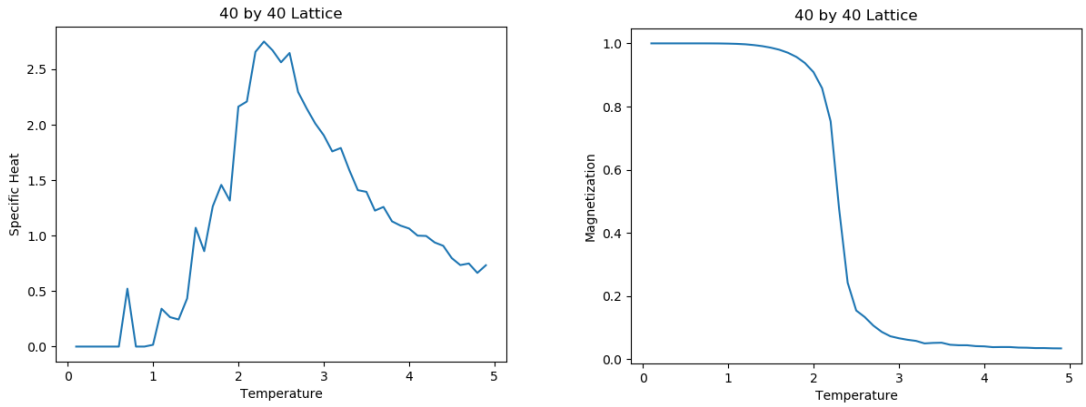

Figure 3: Specific heat and magnetization in a 40 by 40 lattice.

- As expected, the critical (transition) temperature is around 2.5 K.
- The specific heat reaches a peak at T_c.

- The magnetization undergoes a sharp transition from magnetized to demagnetized at the critical temperature. The transition becomes sharper as we increase the lattice size.

2.2 Ground State of Harmonic Oscillator using Variational Monte Carlo

The Hamiltonian of a 1D quantum harmonic oscillator is given by

$$H = -\frac{d^2}{dx^2} + \frac{x^2}{2} \tag{8}$$

This system has a fully analytic solution; however we will solve this using the variational Monte Carlo method.
We use the trail wave function $\Phi(x) = e^{-\alpha x^2}$. The local energy is given by $E_L = \frac{H\Phi}{\Psi} = \alpha + x^2(\frac{1}{2} - 2\alpha^2)$.
By the Metropolis algorithm, the transition probability from x to x' is

$$P_a = \begin{cases} 1 & \text{if } |\Psi(x)|^2 < |\Psi(x')|^2 \\ \frac{|\Psi(x')|^2}{|\Psi(x)|^2} & \text{if } |\Psi(x)|^2 > |\Psi(x')|^2 \end{cases} \tag{9}$$

By performing Monte Carlo sweeps of the positions of the walkers, we determine the average energy of the system. We then vary the parameter α in order to determine the best wave function minimum energy. The error is determined as $\sqrt{\frac{\langle E^2\rangle - \langle E\rangle^2}{NW}}$, where N is the number of steps and W is the number of walkers.

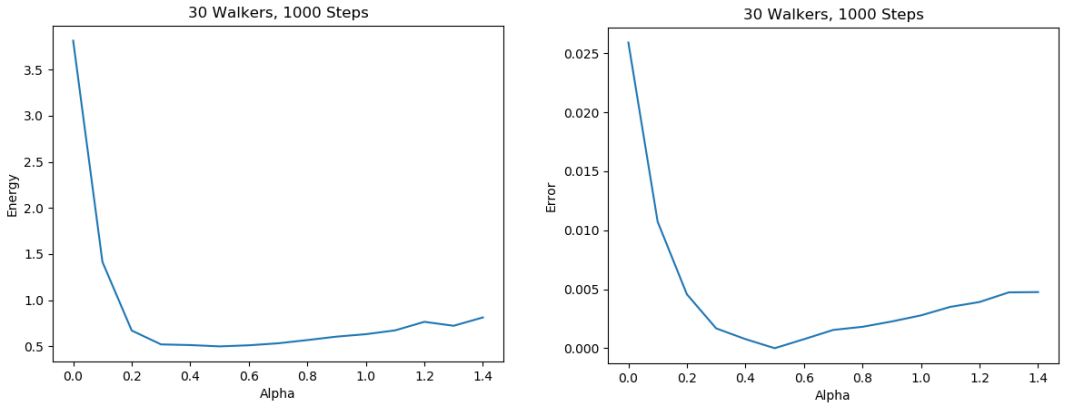

Figure 4: Energy and error for 1000 steps with 30 walkers.

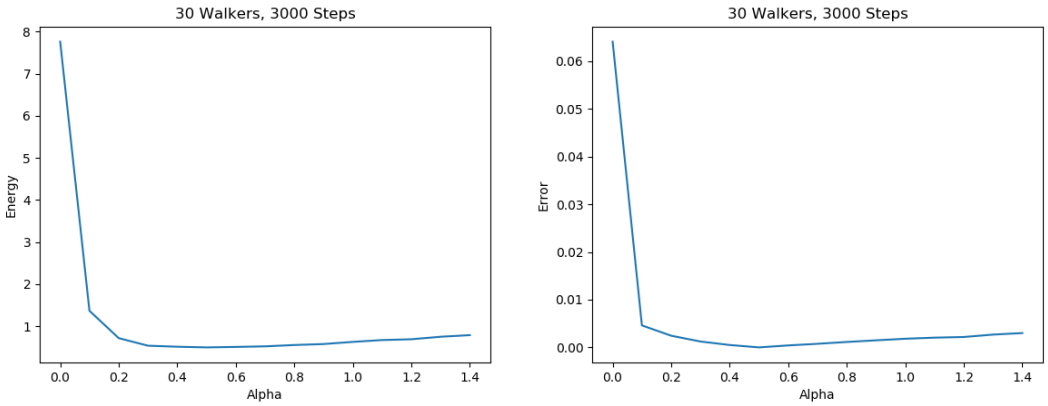

Figure 5: Energy and error for 3000 steps with 30 walkers.

We observe:

- The minimum energy and error occurs at $\alpha = 0.5$. The corresponding wave function is given by $\Psi = e^{-0.5x^2}$, and the energy is $E = 0.5$ (in normalized units).
- This happens to be the exact solution of the harmonic oscillator ground state. It is confirmed by noting that the error is 0 at $\alpha = 0.5$.
- The rate of convergence improves significantly as we increase the number of Monte Carlo steps.

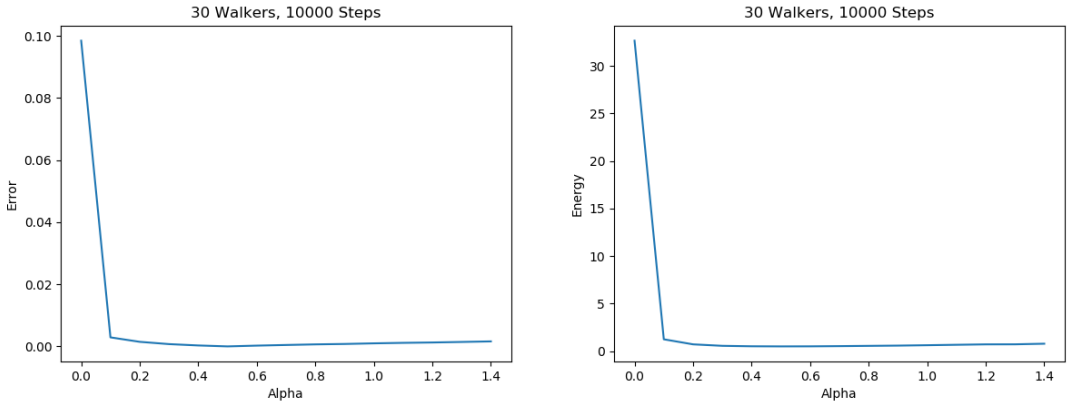

Figure 6: Energy and error for 10000 steps with 30 walkers.

2.3 Ground State of Helium Atom Using Variational Monte Carlo

The Hamiltonian of the helium atom is given by

$$H = -\frac{1}{2}\left(\nabla_1^2 + \nabla_2^2\right) - \frac{2}{r_1} - \frac{2}{r_2} + \frac{1}{r_{12}} \tag{10}$$

We expect the wave function to be similar to the wavefunctions of two electrons in the ground state of hydrogen. Therefore, we select our trail wavefunction as $\Psi = e^{-\alpha(r_1+r_2)}$. The local energy is

$$E_L = \frac{H\Psi}{\Psi} = -\alpha^2 + \frac{\alpha}{r_1} + \frac{\alpha}{r_2} - \frac{2}{r_1} - \frac{2}{r_2} + \frac{1}{r_{12}} \tag{11}$$

The metropolis algorithm is implemented, in order to find the best value for α and the corresponding ground state energy.

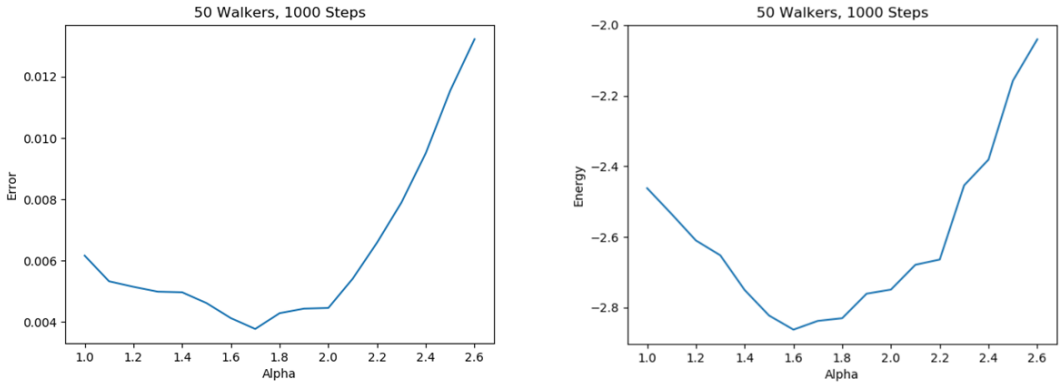

Figure 7: Energy and error for 1000 steps with 50 walkers.

We note:

- The minimum is found at $\alpha = 1.7$, with the corresponding energy around -2.85 Hartrees. This is very close to the experimental value of -2.89 Hartrees.
- By using more and more precise trail wave functions, the ground state energy can be made to converge on the experimental value. For example, our trail wave function does not take into account electron-electron repulsion.
- We also note that even at $\alpha = 1.7$, the error is not equal to 0. This confirms that it is not the exact solution of the system (no exact solution for the Helium atom has been found).

3 Scattering by an Attractive-Repulsive Potential

We model a scattering process with a potential which is repulsive at large distances but attractive at small distances. That is, if the particle gets over a potential hump, it gets stuck inside the well.

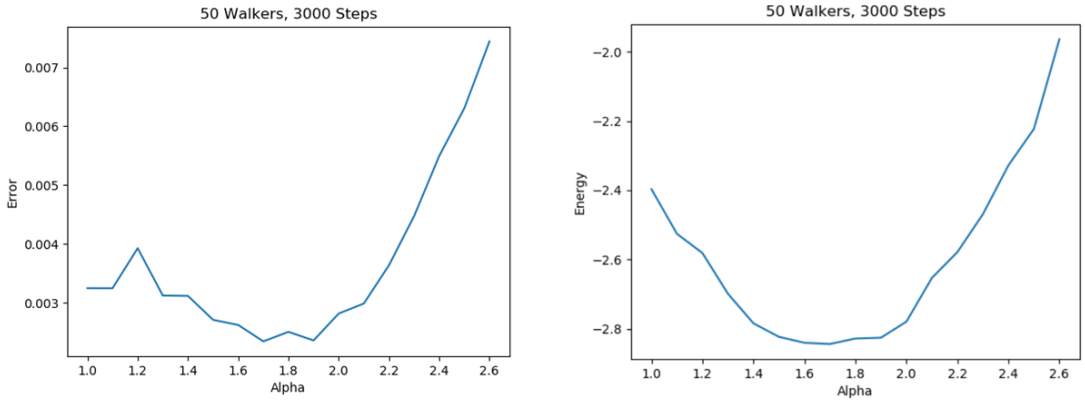

Figure 8: Energy and error for 3000 steps with 50 walkers.

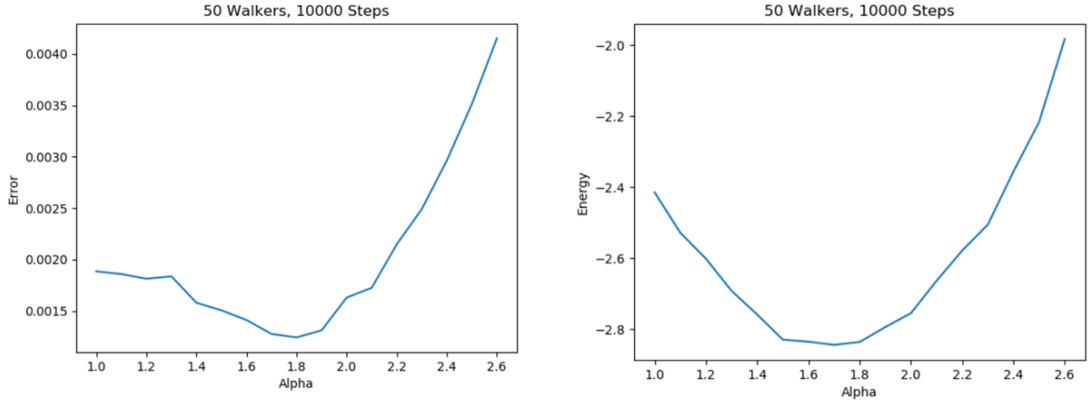

Figure 9: Energy and error for 10000 steps with 50 walkers.

We take

$$V(r) = \frac{1}{r} - \frac{1}{r^2} \tag{12}$$

The Hamiltonian is

$$H = -\frac{1}{2}\nabla^2 + \frac{1}{r} - \frac{1}{r^2} \tag{13}$$

The trail wavefunction has three components:

- A plane wave component in the positive r direction: e^{ikr}
- A growing component: $e^{\beta r}$
- A decaying component: $e^{-\alpha r}$

The full wavefunction is $\Psi = e^{ikr} + e^{\beta r} + e^{-\alpha r}$. The probability density and local energy are given by

$$|\Psi|^2 = e^{-2\alpha r} + e^{2\beta r} + 2e^{2(\beta-\alpha)r} + 2e^{-\alpha r}\cos(kr) + 2e^{\beta r}\cos(kr) + 1 \tag{14}$$

$$E_L = \frac{H\Psi}{\Psi} = \frac{1}{r} - \frac{1}{r^2} - \alpha^2 - \beta^2 + k^2 \tag{15}$$

The energy and error in as a function of α and β are plotted in figure 10. There is an absence of a well defined minimum in the error and energy graphs. This is probably because of the unbounded nature of the potential close to the origin. The choice of wave function must be improved in order to achieve better results; this deserves a separate study.

4 Discrete Dipole Approximation

4.1 Brief Overview

The discrete dipole approximation (DDA) is a technique used to compute the scattering and absorption properties of various materials. The principle of the DDA is to approximate a continuum target by a finite array of polarizable points. These points acquire dipole

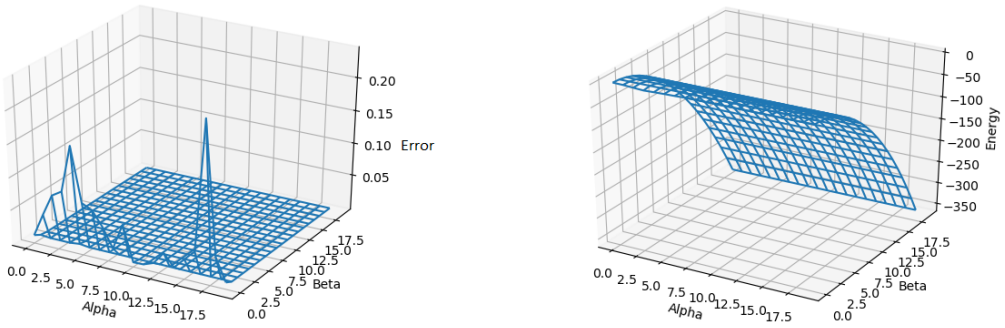

Figure 10: Energy and error for scattering potential.

moments in response to the local electric field. They therefore interact with each other via dipole-dipole forces. Our task is to compute the polarizations of each other dipoles, and use that to find the dielectric function and the polarizability of the material.
Let the target array of point dipoles (labeled with j=1,...,N) be located at points r_j. Each dipole has a polarization $P_j = \alpha_j E_j$, where E_j is the local electric field at r_j and α_j is the polarizability at that point. The local electric field is the sum of contributions of the electric field due to the incident electromagnetic wave and the polarizations of the other $N-1$ dipoles:

$$\begin{aligned} E_{inc,j} &= E_o exp(i\mathbf{k}\cdot\mathbf{r_j} - i\omega t) \\ E_{pol,j} &= -\sum_{k\neq j} A_{jk} P_k \\ E_j &= E_{inc,j} + E_{pol,j} \end{aligned}$$

where A_{ij} are the matrix elements, given by

$$A_{ij} = \frac{e^{ikr_{jk}}}{r_{jk}} \times \left[k^2 (n_{jk} n_{jk} - \mathbf{1_3}) + \frac{ikr_{jk} - 1}{r_{jk}^2} (3 n_{jk} n_{jk} - \mathbf{1_3}) \right]$$

where, k is the wave vector $k = \omega/c$, $r_{jk} = |r_j - r_k|$, and n_{jk} is the unit vector along $r_j - r_k$.
We therefore have a set of 3N complex linear equations to solve for the polarizations P_k:

$$\sum_{k=1}^{N} A_{jk} P_K = E_{inc,j}$$

In matrix form, this is equivalent to solving for P:

$$P = A^{-1} E$$

which can be solved by various numerical methods.
The diagonal elements of the matrix A are related to the isotropic polarizabilities by $A_{jj} = \alpha_J^{-1}$.
Once we have the α_j's, we can solve for the dielectric function of the material using the Clausius-Mossotti relation:

$$\alpha_j = \frac{3d^3}{4\pi} \frac{\epsilon_j - 1}{\epsilon_j + 2}$$

where d is the lattice unit distance.

DDSCAT (Discrete Dipole Scattering) is a FORTRAN code which implements DDA. It was developed jointly by Draine and Flatau and is used for calculating scattering and absorption of light by irregular particles and periodic arrangement of irregular particles. I use DDSCAT to calculate the various quantities of interest of different materials.

4.2 Results

The plots of refractive index (real and imaginary), dielectric function (real and imaginary), and efficiency (scattering, absorption, and extinction) for various materials as a function of wavelength are shown in figures 11-16.

4.3 Size effect

We observe the change in efficiency of extinction across wavelengths as a function of the lattice size. The extinction, absorption, and scattering cross sections are plotted as a function of wavelength for different lattice sizes in figures 17-21. It is clear that at all wavelengths, the extinction and absorption cross sections decrease with increasing size of the lattice, while the scattering cross section increases. The effect is prominent at lower wavelengths.

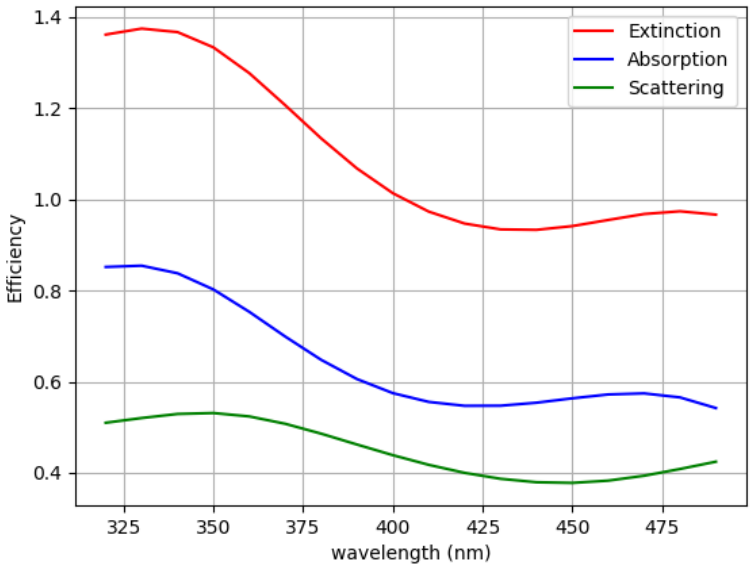

Figure 11: Copper cross sections

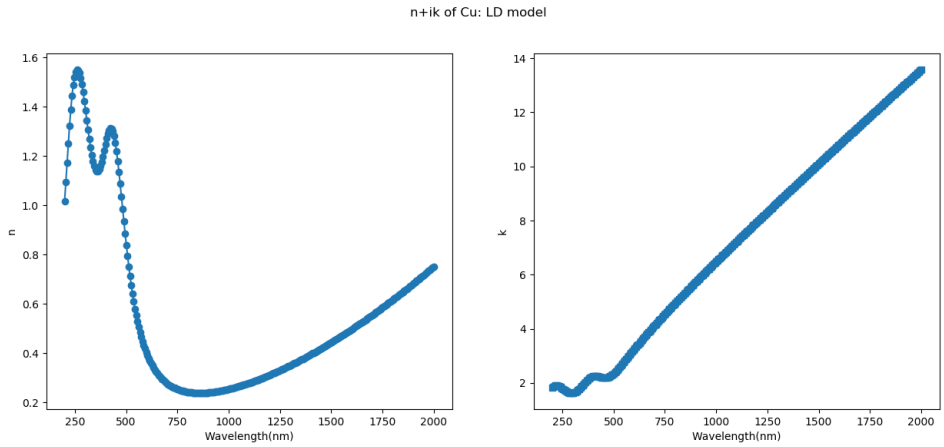

Figure 12: Copper refractive index

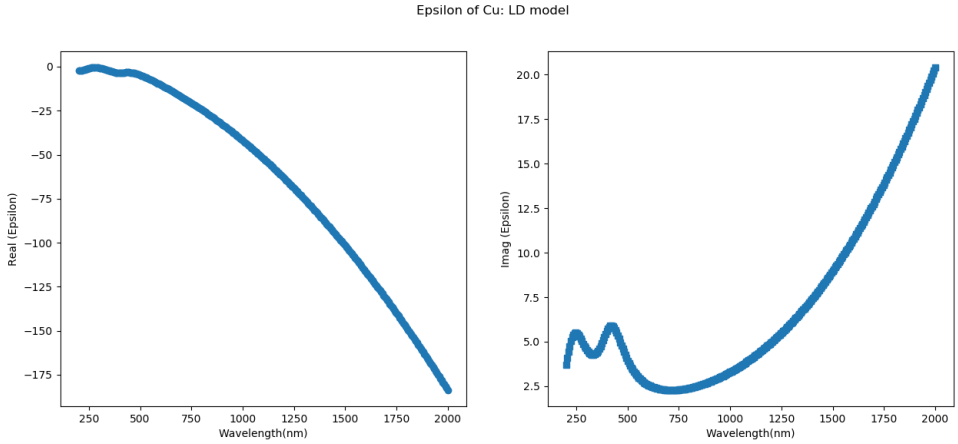

Figure 13: Copper dielectric function

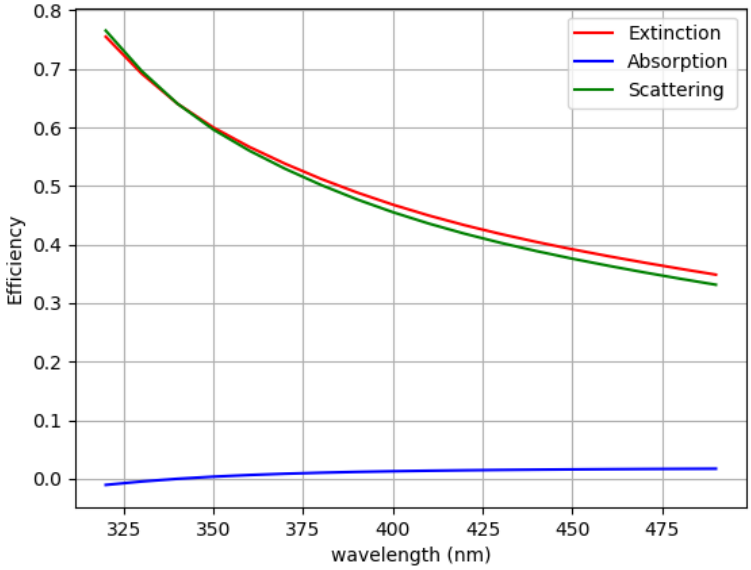

Figure 14: Aluminum cross sections

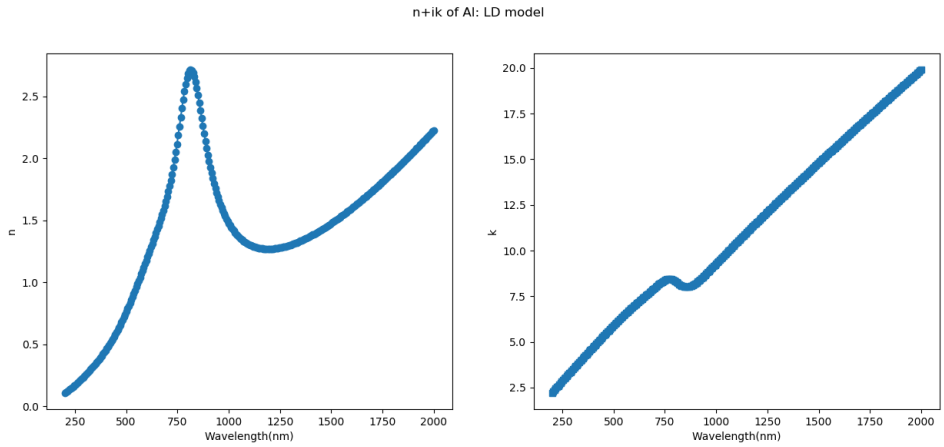

Figure 15: Aluminum refractive index

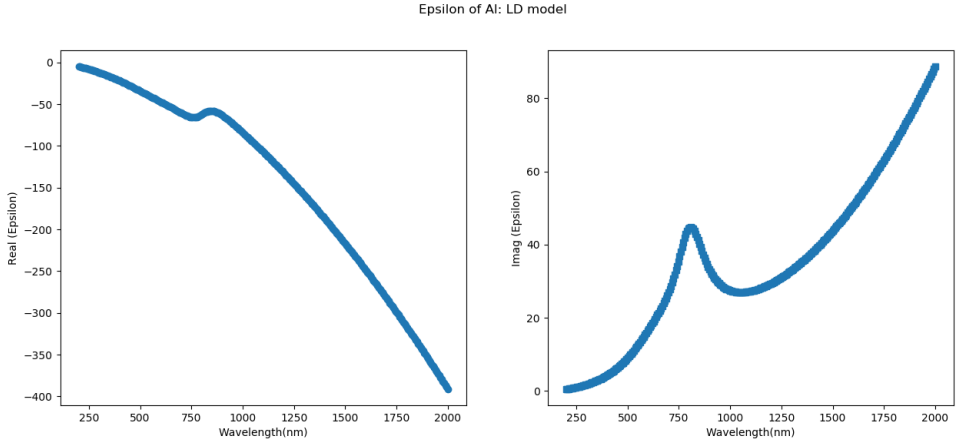

Figure 16: Aluminum dielectric function

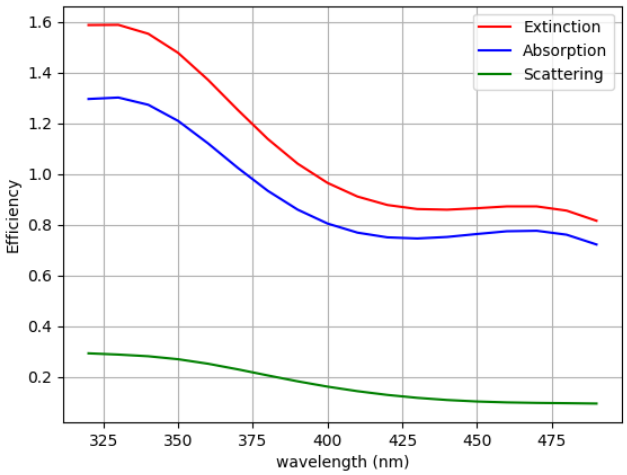

Figure 17: 2x2 lattice

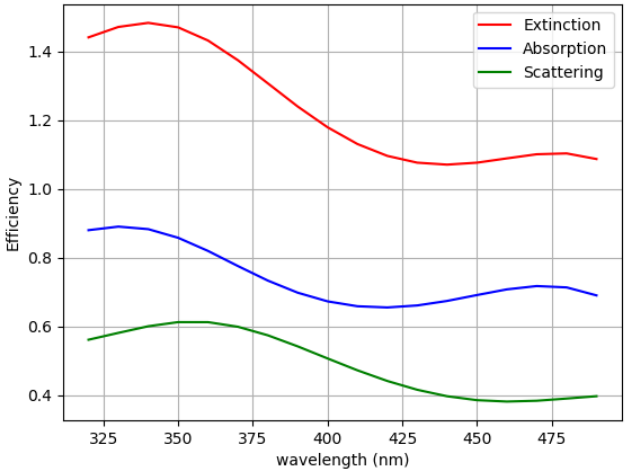

Figure 18: 5x5 lattice

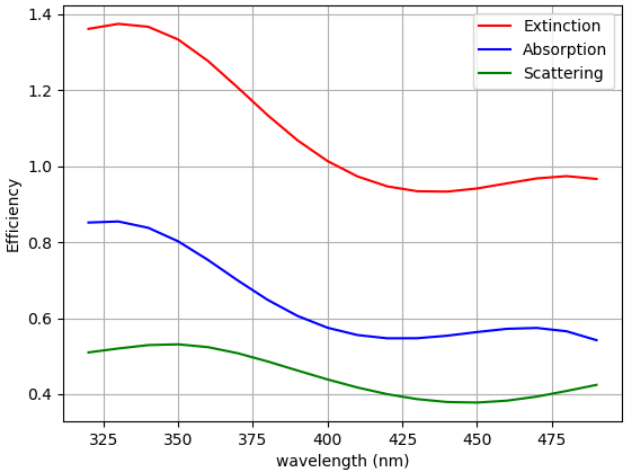

Figure 19: 10x10 lattice

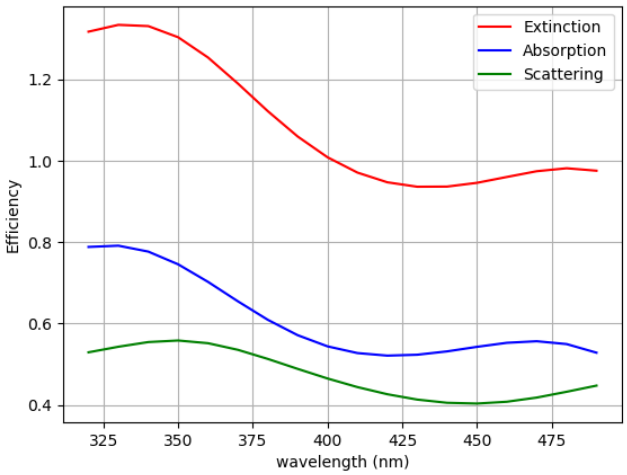

Figure 20: 20x20 lattice

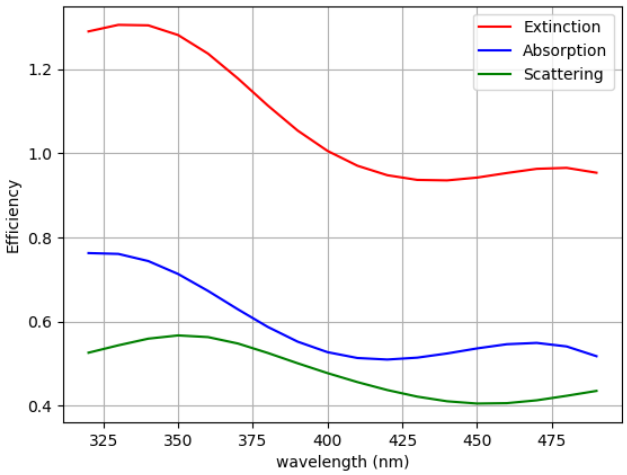

Figure 21: 40x40 lattice

5 Comparision with Mie Theory

Mie theory refers to the analytic solution to the Maxwell equations for scattering off of a homogeneous sphere.

5.1 Theory

We begin with the Maxwell's equations, for wave with time dependance $e^{-i\omega t}$.

$$\nabla \times H = (\sigma - i\omega\epsilon)E = -\frac{i\omega n^2 c^2}{\mu}E \tag{16}$$

$$\nabla \cdot H = 0 \tag{17}$$

$$\nabla \times E = i\omega\mu H \tag{18}$$

$$\nabla \cdot E = 0 \tag{19}$$

with $n = \frac{\sqrt{(\epsilon + i\sigma/\omega)\mu}}{\sqrt{\epsilon_0\mu_0}}$ and $c = \frac{1}{\sqrt{\epsilon_0\mu_0}}$.
We can combine the equations to obtain the scalar wave equation:

$$\nabla^2\Psi - \frac{n^2}{c^2}\frac{\partial^2\Psi}{\partial^2 t} = 0 \tag{20}$$

Substituting for the time dependence,

$$\nabla^2\Psi + k^2\Psi = 0 \tag{21}$$

We define three new vectors L, M, and N such that

$$L = \nabla\Psi \tag{22}$$

$$M = \nabla \times (r\Psi) \tag{23}$$

$$N = \frac{1}{k}\nabla \times M \tag{24}$$

The solution to equation 21 in spherical coordinates is

$$\Psi_{lm}(r) = z_l(kr)P_l^m(\cos\theta)^{\cos m\phi}_{\sin m\phi} \tag{25}$$

We can use this to express the r, θ, and ϕ components of L, M, and N in terms of Ψ.
The electric and magnetic fields can be expressed in terms of a vector potential A:

$$E = -\frac{\partial A}{\partial t} - \nabla\Phi \qquad H = \nabla \times A \tag{26}$$

where

$$A = \frac{i}{\omega}\sum_{l,m}(a_{ml}M_{ml} + b_{ml}N_{ml} + c_{ml}L_{ml}) \tag{27}$$

The electric and magnetic fields are given by

$$H = -\frac{k}{-i\omega\mu}\sum_{l,m}(a_{ml}N_{ml} + b_{ml}M_{ml}) \tag{28}$$

$$E = -\sum_{m,m}(a_{ml}M_{ml} + b_{ml}N_{ml}) \tag{29}$$

The incident fields are taken as

$$E^i = e_x e^{ik_z z} \qquad H_i = e_y e^{ik_z z} \tag{30}$$

Converting to polar coordinates, we see that only the $m = 1$ ters contribute, due to ortholonality.
In addition, we have the boundary condition

$$r \to \infty : z_l(k_z r) = j_l(k_z r) \tag{31}$$

We also have the continuity equations at the surface of the sphere:

$$e_r \times (E^i + E^r) = e_r \times E_t \tag{32}$$

$$e_r \times (H^i + H^r) = e_r \times H^t \tag{33}$$

This allows us to solve for a_l and b_l:

$$a_l^r = -\frac{\Psi_l(y)\Psi_l'(x) - n\Psi_l'(y)\Psi_l(x)}{\Psi_l(y)\zeta_l'(x) - n\Psi_l'(y)\zeta_l(x)} \tag{34}$$

$$b_l^r = -\frac{\Psi_l(x)\Psi_l'(y) - n\Psi_l'(x)\Psi_l(y)}{\Psi_l'(y)\zeta_l(x) - n\Psi_l(y)\zeta_l'(x)} \tag{35}$$

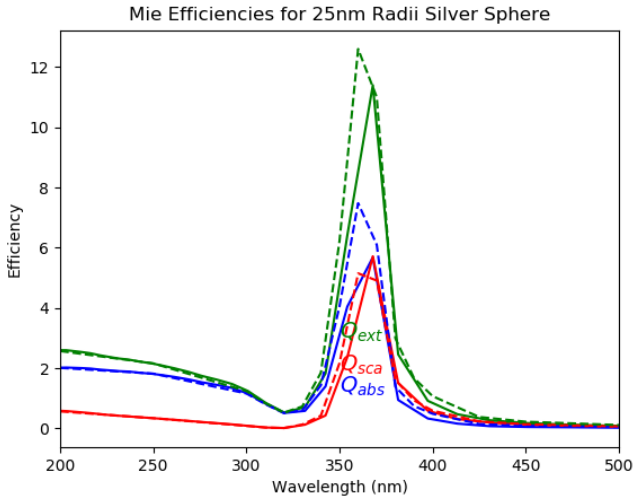

Figure 22: 23 nm silver sphere

where $x = k_2 a$ and $y = k_1 a = n k_2 a$, and $\zeta_l(x)$ is the Riccati-Bessel function.
The outside scattered (reflected) wave is:

$$E^r \sim \sum_{l=1}^{\infty} i^l \frac{2l+1}{l(l+1)} \left(a_l^r M_{1l}^o - i b_l^r N_{1l}^e\right) \tag{36}$$

$$H^r \sim \sum_{l=1}^{\infty} i^l \frac{2l+1}{l(l+1)} \left(b_l^r M_{1l}^e + i a_l^r N_{1l}^o\right) \tag{37}$$

whereas the inside scattered (transmitted) wave is:

$$E^t \sim \sum_{l=1}^{\infty} i^l \frac{2l+1}{l(l+1)} \left(a_t^r M_{1l}^o - i b_l^t N_{1l}^e\right) \tag{38}$$

$$H^t \sim \sum_{l=1}^{\infty} i^l \frac{2l+1}{l(l+1)} \left(b_l^t M_{1l}^e + i a_l^t N_{1l}^o\right) \tag{39}$$

The scattering and extinction cross sections are given by

$$Q_s = \frac{2}{x^2} \sum_{l=1}^{\infty} (2l+1) \left(|a_l^2| + |b_l^2|\right) \tag{40}$$

$$Q_e = \frac{2}{x^2} \sum_{l=1}^{\infty} (2l+1) Re(a_l + b_l) \tag{41}$$

5.2 Results

The results of Mie theory are implemented using the Python module miepython. The results are then compared to the results obtained from DDSCAT.
The Mie efficiencies are for spherical nanoparticles of different material and sizes are plotted as solid lines in figures 23-26. The dashed lines are the corresponding results from DDSCAT. We observe that for small radii ($r << \lambda$), the efficiencies follow Rayleigh's law of $I \propto \lambda^{-4}$.
The results of DDSCAT are in good agreement with the solutions of Mie theory.

References

[1] Draine, B.T. and Flatau, P.J., "Discrete dipole approximation for scattering calculations", J. Opt. Soc. Am. A, 11, 1491-1499 (1994)

[2] Draine, B.T. and Flatau, P.J., "Discrete-dipole approximation for periodic targets: theory and tests", J. Opt. Soc. Am. A, 25, 2593-2703 (2008).

[3] P. J. Flatau and B. T. Draine, "Fast near field calculations in the discrete dipole approximation for regular rectilinear grids," Opt. Express 20, 1247-1252 (2012)

[4] Pottorf, S. and Pudzer, A. and Chou, M.Y. and Hasbun, J.E. Eur. J. Phys. 20 (1999) 205–212.

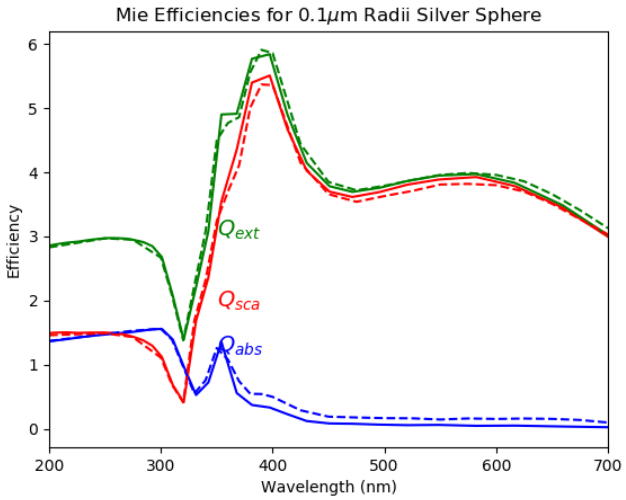

Figure 23: 100 nm silver sphere

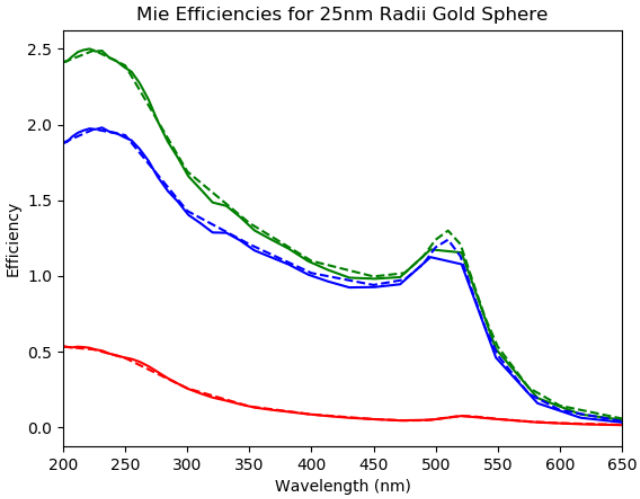

Figure 24: 25 nm gold sphere

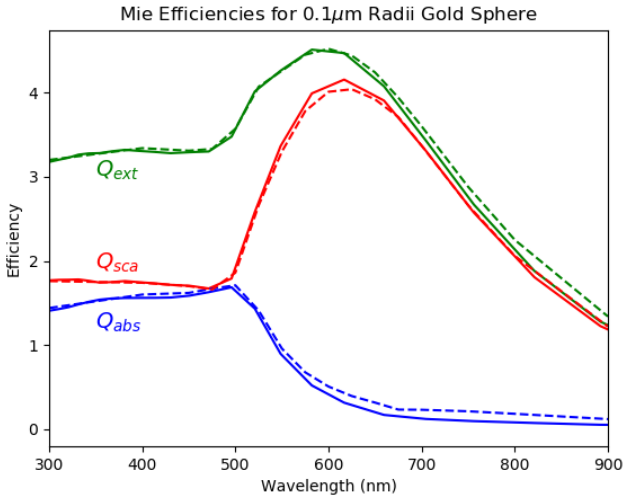

Figure 25: 100 nm gold sphere

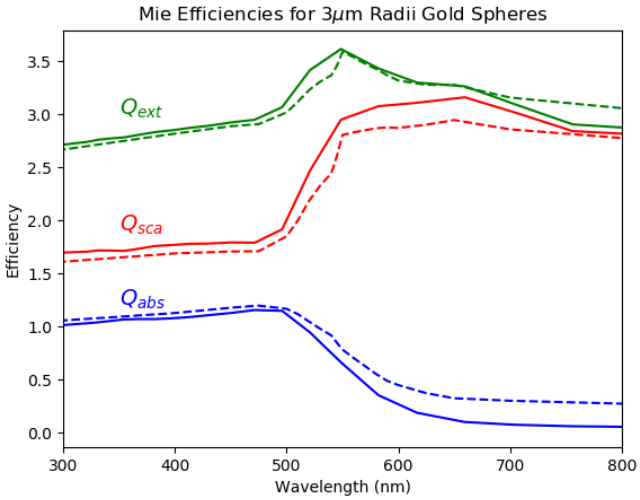

Figure 26: 3 μm gold sphere

[5] Deb, S. "Variational Monte Carlo Technique: Ground State Energies of Quantum Mechanical Systems". Resonance, 19,8: 713-739. 2014.

[6] Ghaforyan, H and Ebrahimzadeh, M and Bilankohi, SM. World appl. programming, Vol(5), No (4), April, 2015. pp. 79-82